FULL PAPER

BJC

British Journal of Cancer (2017) 117, 867–875 | doi: 10.1038/bjc.2017.239

Keywords: cancer-associated fibroblasts; bone; invasion; OSCC; RANKL; stroma; microenvironment

Cancer-associated fibroblasts promote bone invasion in oral squamous cell carcinoma

A A Elmusrati[1], A E Pilborough[1], S A Khurram*[,1] and D W Lambert*[,1]

[1]Unit of Oral and Maxillofacial Pathology, School of Clinical Dentistry, University of Sheffield, Sheffield S10 2TA, UK

Background: The molecular mechanisms involved in the invasion of bone by oral squamous cell carcinomas (OSCC) are poorly understood, and little is known about the role of cancer-associated fibroblasts (CAF), the presence of which confers a poor prognosis.

Methods: Clinicopathological data from 277 OSCC cases involving bone resections were reviewed, and 32 cases thoroughly analysed histologically. Immunohistochemistry was used to examine αSMA, RANKL and OPG. Western blotting and qPCR were used to assess myofibroblast (CAF-like) differentiation, RANKL and OPG expression *in vitro*, and RANKL secretion was analysed by ELISA. Osteoclastogenesis was examined using TRAP staining, multinucleation and pit forming assays.

Results: Fibrous stroma intervened between tumour and bone in the majority of cases, with no direct contact between cancer cells and bone. RANKL and OPG, two proteins key to regulating bone resorption, were expressed in tumour cells as well as fibrous stroma adjacent to bone and αSMA-positive myofibroblastic CAF were consistently seen infiltrating into bone ahead of tumour cells. Human primary osteoblasts cultured with conditioned media from human OSCC-derived cells and human primary CAF showed a significant increase in RANKL and a decline in OPG mRNA expression. RANKL secretion was significantly increased in primary oral fibroblasts induced to differentiate into a CAF-like phenotype by transforming growth factor-β1 (TGF-β1) treatment and in primary CAF. Indirect co-culture of murine macrophages with conditioned media from CAF (experimentally derived and isolated from OSCCs) resulted in a marked increase in osteoclastogenesis (in excess of that provoked by cancer cells) determined by tartrate-resistant acid phosphatase activity, multinucleation and resorption pit formation.

Conclusions: This study is the first to describe a functional role for CAFs in bone invasion and turnover, identifying a novel potential therapeutic target and diagnostic indicator in this difficult to treat bone invasive malignancy.

Oral squamous cell carcinoma (OSCC) is characterised by heterogeneous morphological features and invasion of regional anatomical structures. As the tumour grows it invades the surrounding tissues and can penetrate proximal bone. The presence of bone invasion worsens prognosis and upgrades the tumour stage, with 12–56% of OSCCs presenting with bone invasion (Chen *et al*, 2011). The mechanism by which OSCC invades underlying bone remains unclear, hampering prognosis and the development of improved treatment strategies (Quan *et al*, 2012).

Recently it has become increasingly evident that the tumour associated stroma (predominantly fibroblasts, endothelial cells, inflammatory cells and associated matrix) plays a significant role in tumour progression in OSCC (De Wever *et al*, 2008). Stromal fibroblasts (cancer-associated fibroblasts, CAF) expressing the myofibroblast marker α-smooth muscle actin (αSMA) have been reported in several solid tumours, including OSCC, and their presence is strongly associated with a poor clinical outcome (Radisky *et al*, 2007). Ishikuro *et al*, 2008 demonstrated expression of the osteoclastogenic factors RANK (receptor activator of nuclear factor-kappaB) and its ligand RANKL in OSCC stroma adjacent to bone but the precise role of stromal fibroblasts/CAF in bone invasion remains unknown.

In the present study, we undertook a comprehensive clinical, histopathological, and *in vitro* approach to analyse the contribution

*Correspondence: Dr SA Khurram; E-mail: s.a.khurram@sheffield.ac.uk or Dr DW Lambert; E-mail: d.w.lambert@sheffield.ac.uk

Received 21 April 2017; revised 22 June 2017; accepted 29 June 2017; published online 25 July 2017

of stromal fibroblasts to bone invasive OSCC, and demonstrate for the first time that CAFs promote osteoclastogenesis and are intimately associated with tumour invasion into bone. These findings suggest that interventions targeting the tumour stroma may have promise as a novel therapeutic approach in bone invasive OSCC.

MATERIALS AND METHODS

Case selection. Data from 277 OSCC cases with bone resection was retrieved from the unit archive (1994–2014) and thoroughly reviewed. The assessed criteria included those laid out in the Royal College of Pathologists (RCPath) minimum data set such as site of primary tumour, grade of tumour (well, moderate and poorly differentiated), pattern of invasive front (cohesive and discohesive), presence or absence of bone invasion, depth of bone invasion (cortical or cancellous), lymph node metastasis, lymphovascular invasion and perineural infiltration (Supplementary Table S1).

Histological analysis. Paraffin-embedded sections (4 μm) were obtained from 37 samples including 32 OSCCs with bone invasion and five bone invasive ameloblastomas (locally aggressive odontogenic epithelial tumour with direct infiltration into bone) for comparison. These cases were selected as being representative of the entire cohort, with both maxillary and mandibular cases, as well as cases showing cortical and cancellous invasion, included, and with sufficient interface tissue available for analysis and immunohistochemistry. Haematoxylin and eosin (H&E) and martius scarlet blue (MSB) staining were carried out and histologically evaluated (Supplementary Table S2). Depth of tumour invasion in relation to underlying bone was examined and characterised as cortical/superficial or cancellous/deep bone marrow infiltration. Grade of OSCCs was assessed based on Broder's classification, and the tumours were graded as well, moderate or poorly differentiated (Roland *et al*, 1992). The pattern of tumour advancement was classified as cohesive or discohesive using the recommended guidelines (Müller and Slootweg, 1990). Host response was determined as strong, moderate or poor (abundance of lymphocytic infiltration) in the tumour microenvironment at the site of bone invasion (Supplementary Table S2). Tumour and bone interface was also inspected for presence or absence of fibroblastic stroma (loose myxoid-like appearance comprising scanty collagen, and fibroblasts with fusiform nuclei). The number of osteoclasts (large multinucleated cells in bone lacunae, detected in three random high-power magnification fields $\times 40$) at tumour-bone interface was also quantified (Supplementary Table S3).

Immunohistochemical analyses. Immunohistochemistry was carried out on matched cases of cortical ($n=5$), cancellous ($n=5$) bone invasive OSCC resections and amelobastoma/control cases ($n=5$) (total = 15 cases). Immunohistochemistry for OPG, RANKL and αSMA was performed as previously described (Khurram *et al*, 2010) using the avidin-biotin peroxidase complex (ABC) method (ethical approval 07/H1309/150). Tissue sections were deparaffinised in xylene (10 min), and rehydrated in absolute alcohol (10 min). Sections were incubated with 3% (v/v) hydrogen peroxide in methanol (20 min) to eliminate endogenous peroxidase activity, and subsequently briefly rinsed in phosphate-buffered saline (PBS). Heat-induced epitope retrieval was conducted for all antibodies by microwaving in 0.01 M tri-sodium citrate buffer (pH 6) for 5 min, and cooled for 3 min to avoid detachment of bone tissue. After washing with PBS, blocking serum (100% horse serum for mouse antibodies, and 100% goat serum for rabbit antibody) was applied to sections for 30 min at room temperature (RT). Tissue sections were incubated with rabbit anti-human RANKL polyclonal antibody (anti-RANKL antibody ab9957; abcam, Cambridge, UK; 1:50), rabbit anti-human OPG polyclonal antibody (anti-osteoprotegrin antibody ab73400; abcam; 1:100) diluted in 100% goat serum, mouse anti-human αSMA monoclonal antibody (monoclonal anti-actin, α-smooth muscle antibody A5228; Sigma-Aldrich, Poole, UK, 1:200) diluted in 100% horse serum, overnight at 4 °C in a humidified chamber. Unbound primary antibody was removed by washing in PBS followed by addition of secondary biotinylated antibodies at RT for 30 min in accordance with the manufacturer's instructions (Vectastain Elite ABC Kits, Vector Laboratories, Burlingame, CA, USA). ABC solution was applied for 30 min at RT and the slides washed in PBS. Nova Red Peroxidise substrate kit (Vector Laboratories) was used as a chromogen, sections were counterstained with Harris's haematoxylin (Thermo Electron Corporation, Loughborough, UK) and mounted in DPX. Staining intensity/percentage was quantified in five random fields per section at the tumour-bone interface using an Automated Cellular Imaging System (ACIS III, Agilent, Santa Clara, CA, USA).

Cell culture. Human primary osteoblasts HOB (passage 2) were kindly provided by Dr Keyvan Moharamzadeh (Sheffield Research Ethics Committee Ref. 15/LO/0116, STH18551). The OSCC-derived cell line H357 was obtained from ATCC (Manassas, VA, USA), and primary human oral fibroblasts (passage 7–8) were isolated as previously described (Hearnden *et al*, 2009). Human primary CAFs were isolated from fresh tissue derived from patients with OSCC undergoing resections within the hospital (Sheffield Research Ethics Committee Ref. 13/NS/0120, STH17021; CAF 002, 003 and 004, kindly provided by Amy Harding and Dr Helen Colley), (Kabir *et al*, 2016). The murine macrophage cell line (RAW 264.7) was acquired from ATCC (ATCC, TIB-71), and used at passage 6.

HOB and H357 cell lines were cultured and maintained in DMEM containing 10% (v/v) foetal calf serum, penicillin/streptomycin (100 i.u.ml and 100 $\mu g\,ml^{-1}$, respectively), 2 mM L-glutamine, and fungizone (250 $\mu g\,ml^{-1}$), while primary normal fibroblasts and CAF were maintained in DMEM containing 10% (v/v) foetal calf serum and 2 mM L-glutamine. RAW 264.7 cells were cultured in DMEM supplemented with 10% (v/v) foetal calf serum and penicillin/streptomycin (100 i.u.ml and 100 $\mu g\,ml^{-1}$). All cells were grown in T75 cm^2 flasks, maintained in a 99% humidified incubator at 37 °C in 5% CO_2, and cultured until 70–80% confluence.

Culture of osteoblasts with conditioned media of H357 or CAF 003 and 004 was performed by seeding osteoblasts (250 000–500 000 cells) into six-well plates. Cells were allowed to adhere overnight followed by serum starvation for 24 h. Osteoblasts were incubated with conditioned media from H357 OSCC-derived cancer cells, experimentally derived CAF or OSCC-derived CAF for 24 h. Osteoblasts cultured with serum-free media served as a negative control. Finally, cells were lysed and RNA extraction was performed immediately.

Quantitative real-time PCR (qPCR). Total RNA was extracted from cultured cells using RNeasy Mini Kit (Qiagen, Crawley, UK) and reverse transcribed to complementary DNA (cDNA) using a High Capacity cDNA Reverse Transcription Kit (Applied Biosystems, Thermo Fisher, Loughborough, UK). Following reverse transcription the samples were subjected to Taqman qPCR analysis (7900HT Fast Real Time PCR System; Life Technologies, Thermo Fisher, Loughborough, UK). The Taqman primers (Life Technologies) used for amplification were as follows: RANKL (TNFSF11, part no. Hs00243522_m1), OPG (TNFRSF1, part no.Hs00900358_m1). αSMA transcripts were detected by SYBR green qPCR (Life Technologies) using the following primers: αSMA Forward 5′ GAAGAAGAGGACAGCACTG 3′, αSMA Reverse 5′ TCCCATTCCCACCATCAC 3′ U6 Forward 5′

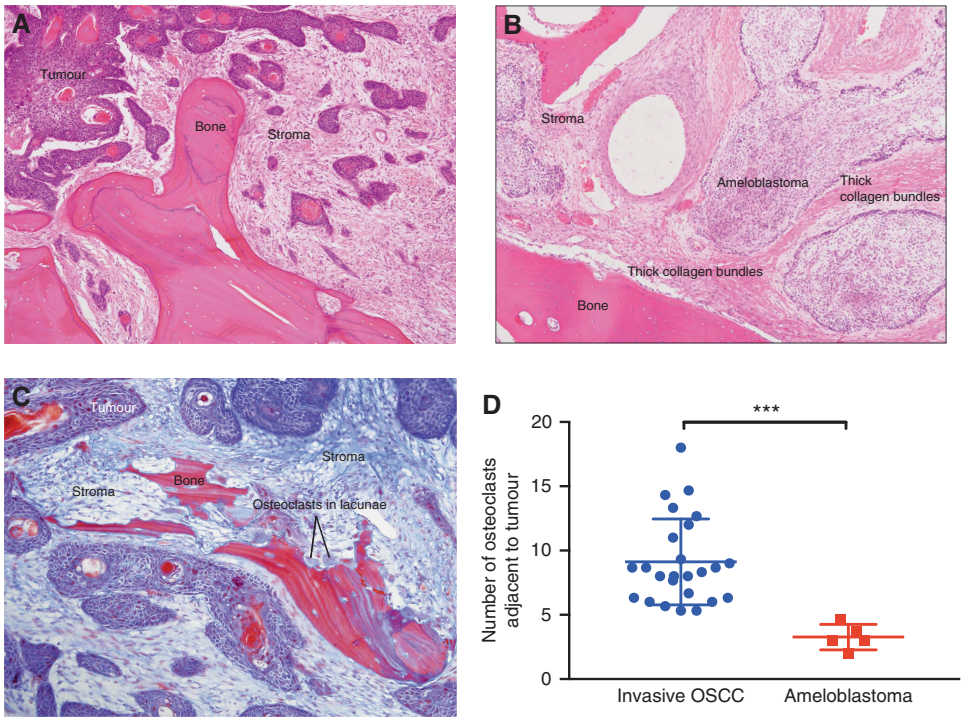

Figure 1. Prevalent stromal presence in bone invasive OSCC. Photomicrographs of MSB and H&E stained bone invasive OSCC and ameloblastoma tissue sections. (**A**) Abundant stroma in OSCC microenvironment, and extending into bone (H&E staining × 10). (**B**) Fibrous tissue, and thick collagen bundles surrounding ameloblastoma (H&E staining × 10). (**C**) OSCC tumour islands and fibrous stroma invading bone, osteoclasts evident in lacunae on bone resorptive surface (MSB staining × 20). (**D**) Number of osteoclasts per high-power field proximal to OSCC was significantly higher than ameloblastoma. Data represent the mean ± s.d. ($n = 3$). ***$P \leqslant 0.001$.

CTCGCTTCGGCAGCACA 3′, U6 Reverse 5′ AACGTTCAC-GAATTTGCGT 3′ (Hinsley *et al*, 2012). Amplification was normalised to U6 (SYBR green) and human B2M (Taqman; part no. 4331182, Life Technologies) in all samples using the Livak method (Livak and Schmittgen, 2001).

Myofibroblast differentiation. Primary normal human oral fibroblasts (NOF) were seeded into six-well plates and serum starved for 24 h. Recombinant human TGF-β1 (5 ng ml^{-1}; R&D Systems, Minneapolis, MN, USA) was added to the cells in serum-free media and cells and medium harvested after 72 h, as previously described (Kabir *et al*, 2016). NOF cultured in serum-free media served as a negative control. Conditioned media was collected and stored at −20 °C in preparation for ELISA.

ELISA for RANKL. A sandwich technique was performed using a DuoSet ELISA development kit (Catalogue number: DY626, R&D Systems), according to the manufacturer's instructions, to detect and quantify RANKL in conditioned medium collected from NOFs, experimentally derived CAF, and OSCC-derived CAFs.

Western blot for αSMA expression. Proteins were extracted from TGF-β1-stimulated oral myofibroblasts with RIPA buffer (20 mM Tris-HCl (pH 7.5), 1 mM EDTA, 50 mM b-glycerophosphate, 150 mM NaCl, 1 mM Na3VO4, 1% NP-40, 25 mM NaF) containing protease and phosphatase inhibitors cocktail (Sigma-Aldrich). The solubilised proteins were resolved using SDS-PAGE and transferred onto polyvinylidene fluoride membranes (ATTO, Tokyo, Japan). Protein identification was performed by western blotting using primary antibodies raised against αSMA (1/1000; Sigma, A5228) and GAPDH (1/5000; Abcam ab185059), diluted in TBS containing 5% dried milk and 3% BSA, followed by secondary antibodies conjugated with horseradish peroxidase. Immunoreactive bands were detected using enhanced chemiluminescence reagents (GE Healthcare; Pittsburgh, PA, USA).

Osteoclastogenesis assays. Macrophage (RAW 264.7) cells (50 000 cells per ml in MEM-Alpha medium (Sigma) were transferred to 24-well Corning Osteo Assay plates (catalogue number- 3988, Corning). Conditioned media from serum starved OSCC cells (H357), CAF, NOF or experimentally derived CAF was collected, filtered using 0.22 μm Millex GP filter unit (Merck Millipore Ltd, IRL, Feltham, UK), and added to the wells. Medium containing recombinant RANKL (rRANKL, 50 ng ml^{-1}; Sigma) served as a positive control. Serum-free differentiation media served as a negative control. The plates were incubated in a 5% CO_2 humidified atmosphere at 37 °C for 7 days with a medium change daily.

To verify osteoclast formation, tartrate-resistant acid phosphatase (TRAP) staining was performed using a TRAP staining kit (B-Bridge International) according to the manufacturer's instructions. Osteoclasts were identified by light microscopy as large TRAP positive multinucleated (three or more nuclei) cells, and quantified in three randomly selected high-power magnification fields (× 40).

Separate wells of the 24 Osteo Assay plate were analysed for osteoclast pit formation. Differentiation media was aspirated after 7 days, and 400 μl of 10% (v/v) sodium hypochlorite was added for 5 min at RT. The wells were washed thoroughly with distilled water and allowed to dry for 5 h. Pits and clusters were observed and quantified using a light microscope (Nikon Eclipse TS-100, Kingston-upon-Thames, UK) in three randomly selected high-power magnification fields.

Fluoro cytochemical detection of multinucleated osteoclasts. RAW 264.7 cells were seeded on coverslips in 24-well plates (50 000 cells per well), and allowed to propagate in differentiation media MEM-Alpha (Sigma) supplemented with 10% foetal calf serum, 1% penicillin/streptomycin and 50 ng ml^{-1} recombinant RANKL (rRANKL; R-0525, Sigma), for 7 days, with a daily media

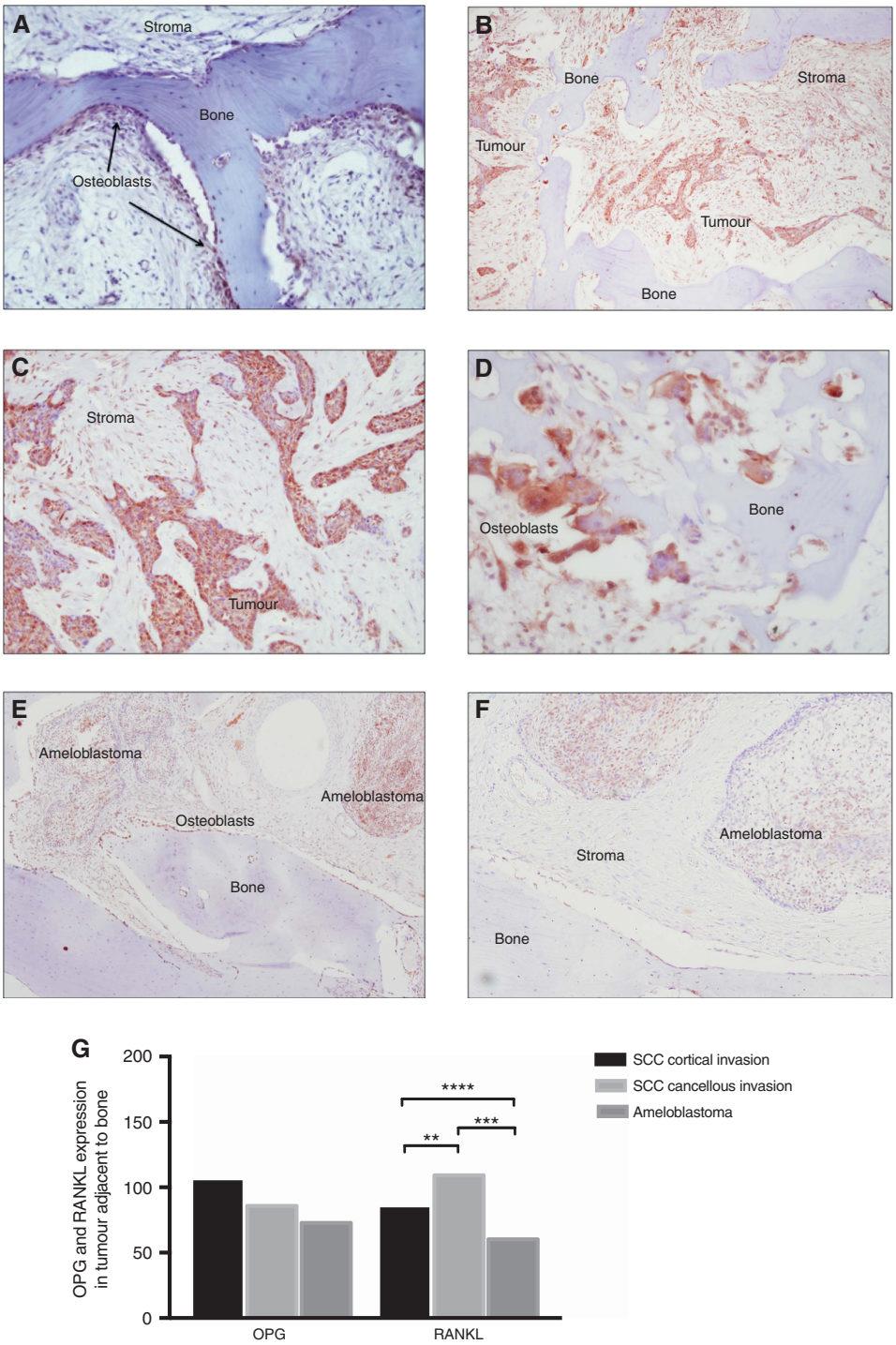

Figure 2. Strong OPG and RANKL expression in OSCC tumour proximal to bone. Representative photomicrographs showing immunohistochemical staining in bone invasive OSCC and ameloblastoma tissue sections. (**A**) Strong cytoplasmic OPG staining in osteoblasts in bone resorptive regions in OSCC (magnification ×10). (**B**) OPG staining in OSCC tumour islands, associated fibrous stroma and osteoclasts (multinucleated cells) (magnification ×10). (**C**) Strong RANKL (antibody dilution 1:50) staining in infiltrative tumour islands (magnification ×20, higher magnification of Figure 2B). (**D**) Pit forming osteoclasts (large cells with three or more nuclei) and surrounding tissue express RANKL on bone resorptive surface (magnification ×40). (**E**) OPG localisation in osteoblasts and weak expression in ameloblastoma stellate reticulum-like cells (magnification ×10). (**F**) Weak RANKL staining in ameloblastoma islands and osteoblasts (magnification ×10). (**G**) Quantification of OPG and RANKL staining intensity with significantly stronger RANKL staining in both cortical and cancellous bone invasive OSCCs compared to ameloblastoma. No significant difference in OPG staining was detected. Data represents mean ± s.d. $^{**}P \leqslant 0.01$; $^{***}P \leqslant 0.001$; $^{****}P \leqslant 0.0001$.

change. Media was removed, washed with PBS, followed by formaldehyde (3.7% formaldehyde in PBS) fixation for 5 min. Cells were then dehydrated in acetone (5 min), and permeabilised with 0.1% Triton X-100 (Sigma) in PBS. After thorough washing in PBS, coverslips were mounted on glass slides using SlowFade Diamond Antifade Mountant containing DAPI (ThermoFisher) as a nuclear counterstain. Images were obtained using a Axioplan 2 fluorescent microscope.

Statistical analysis. Data was expressed as mean ± s.d. Paired Student's *t*-test and Fisher's test was used to determine the

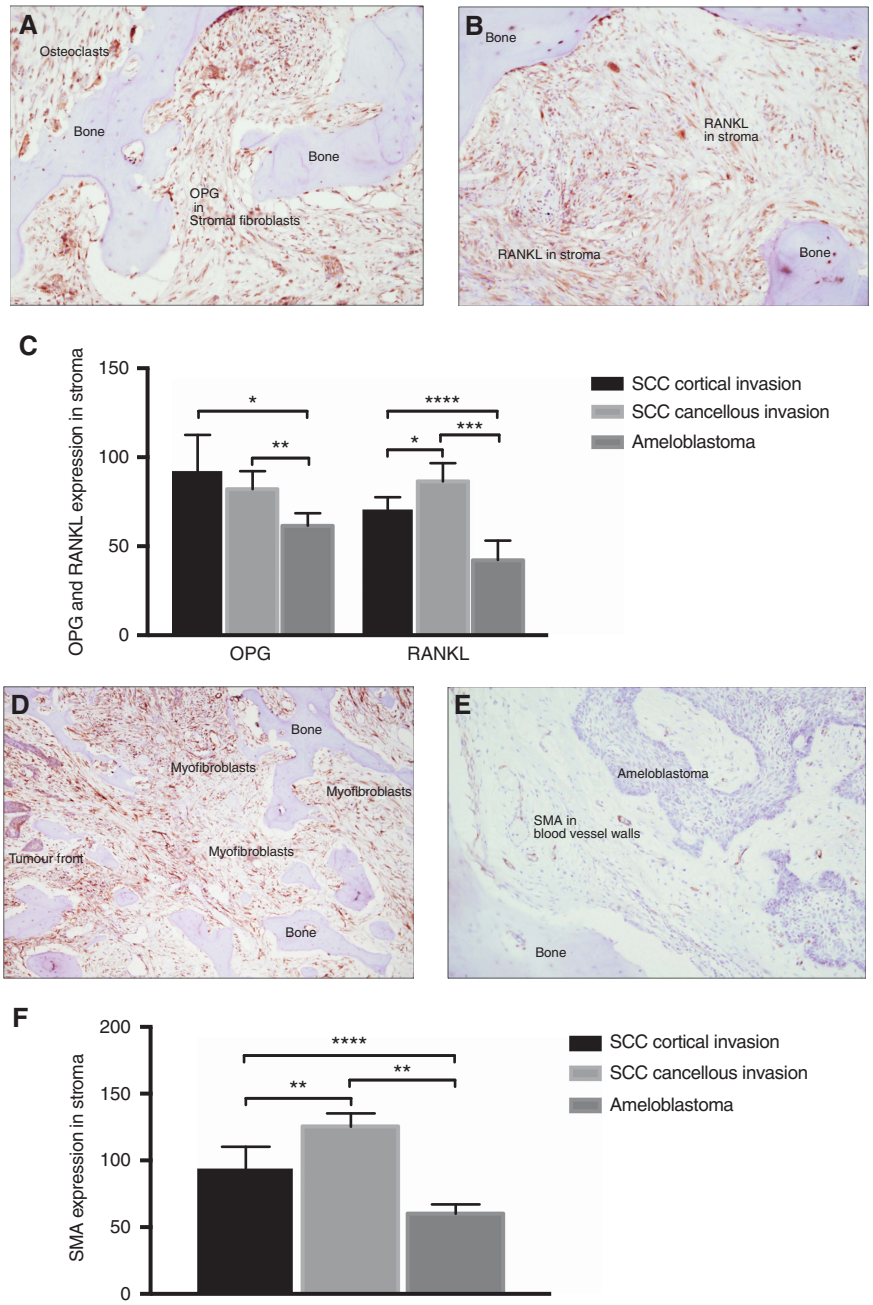

Figure 3. αSMA-positive stromal expression of OPG and RANKL between tumour and bone interface. Representative photomicrographs showing immunohistochemical staining in stroma of bone invasive OSCC and ameloblastoma tissue sections. (**A&B**) OPG and RANKL expression detected in osteoclasts (large multinucleated cells) on bone surface, and intervening fibroblasts. (**C**) Quantification of intensity of OPG and RANKL staining. Data represent the means ± s.d. (**D**) Strong αSMA-positive myofibroblastic stroma at advancing OSCC tumour front invading bone (magnification × 10). (**E**) Weak αSMA expression of blood vessels in ameloblastoma (magnification × 20). (**F**) Quantification of intensity of αSMA expression showed significantly stronger stromal staining in both cortical, and cancellous bone invasive OSCC, compared to ameloblastoma. Data represent the means ± s.d. *$P \leqslant 0.05$; **$P \leqslant 0.01$; ***$P \leqslant 0.001$; ****$P \leqslant 0.0001$.

statistical significance of results where appropriate. A *P*-value of less than 0.05 was considered statistically significant.

RESULTS

The presence of fibrous stroma is a prominent feature of bone invasion. We first investigated the presence or absence of fibrous stroma (indicative of the presence of CAFs) at the tumour-bone interface in bone invasive OSCC (Figure 1A) and compared it to ameloblastoma, a benign tumour of the odontogenic epithelium which frequently infiltrates bone (Figure 1B). An estimated 90.62% ($n = 29/32$) of bone invasive OSCCs presented with identifiable fibrous stroma, compared to only 20% ($n = 1/5$) of ameloblastomas (Figure 1C and Supplementary Table S3). A significantly higher number of osteoclasts were observed at the bone interface in OSCC compared to ameloblastoma ($P < 0.001$) (Figure 1D).

Bone turnover markers are expressed in bone and stromal cells at the tumour-bone interface. Expression of markers associated

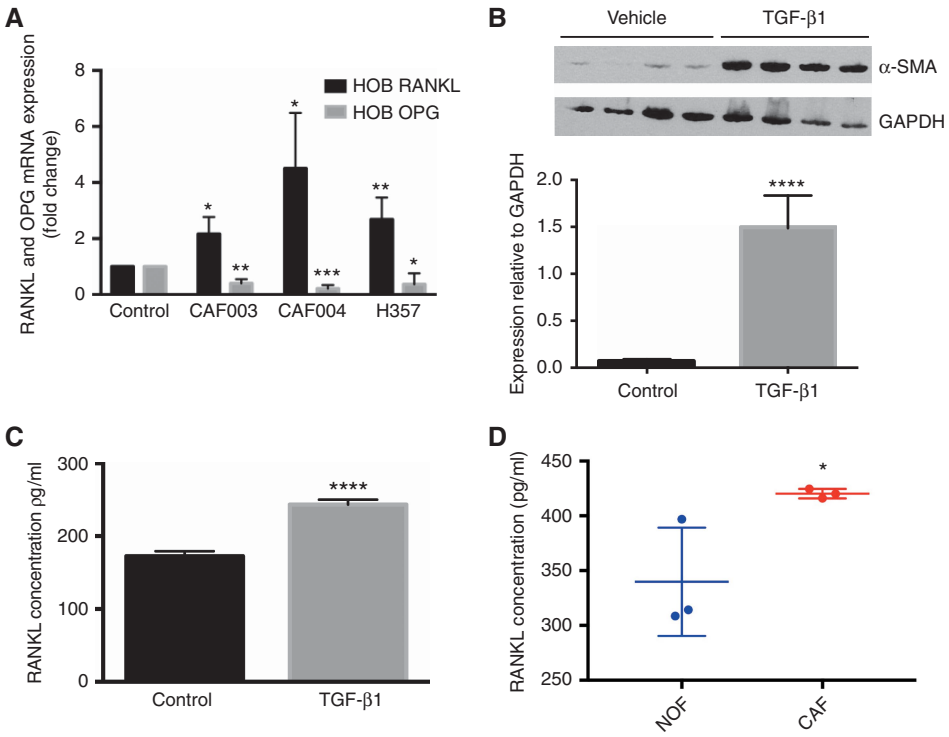

Figure 4. CAFs stimulate expression of RANKL in osteoblasts. (**A**) mRNA expression of OPG and RANKL in human osteoblasts (HOB) following 24 h culture with conditioned media from CAF and H357 cells. Data represent $n = 3 \pm$ s.d. (**B**) Immunoblot of αSMA protein in NOF treated with TGF-β1 (5 ng ml^{-1}) for 72 h. GAPDH was used as a loading control, and densitometry carried out normalised to GAPDH in the same samples (lower). (**C**) Conditioned medium was collected from TGF-β1 treated NOF (72 h treatment) and soluble RANKL quantified by ELISA. (**D**) RANKL was quantified in conditioned medium collected from OSCC-derived CAF (002, 003 and 004). Data represent $n = 3 \pm$ s.d. *$P \leqslant 0.05$; **$P \leqslant 0.01$; ***$P \leqslant 0.001$; ****$P \leqslant 0.0001$.

with bone remodelling was analysed using IHC in selected matched cases ($n = 15$). Cytoplasmic staining of OPG and RANKL was evident in osteoblasts and osteoclasts as well as tumour cells proximal to bone (Figure 2A–D). Interestingly, the staining intensity appeared to gradually weaken in OSCC cells further away from bone (Figure 2A–D). In ameloblastomas, weak OPG and RANKL immunoreactivity was seen in the inner stellate reticulum-like cells only (Figure 2E and F). RANKL staining was significantly stronger in both cancellous and cortical OSCC bone invasion ($P < 0.001$ and $P < 0.00001$ respectively) than ameloblastoma, while levels of OPG immunoreactivity were similar (Figure 2G).

Both OPG and RANKL staining was also consistently observed in fibrous stroma between tumour and bone, and particularly surrounding osteoclasts in active bone resorptive sites (Figure 3A and B). Although the intensity of expression varied between the OSCC cases, only weak staining was observed in ameloblastomas (data not shown). Stromal staining for RANKL and OPG expression was significantly stronger in OSCC exhibiting either cortical or cancellous bone invasion ($P < 0.01$) than ameloblastoma (Figure 3C).

Strong αSMA immunoreactivity was seen in fibrous stroma at the tumour and bone interface, and surrounding osteoclasts, in bone resorptive areas (Figure 3D), indicative of the presence of CAF. Moreover, in several cases, αSMA-positive CAF were observed infiltrating bone ahead of the epithelial tumour cells (Figure 3D). Stromal αSMA staining proximal to bone was significantly stronger in OSCC than ameloblastoma ($P < 0.002$ cortical and $P < 0.00005$ cancellous) (Figure 3E and F).

Human OSCC cells and CAFs enhance RANKL expression and reduce OPG mRNA in human primary osteoblasts. Bone remodelling depends upon a tightly regulated balance between osteoblast-mediated bone deposition and osteoclastic bone resorption. Osteoclastic effects of RANKL are constrained by the presence of its decoy receptor, OPG, both of which are secreted by osteoblasts. To investigate the effect of OSCC-cell-derived factors on OPG and RANKL expression in osteoblasts, HOB primary human osteoblasts were cultured in H357 (an OSCC-cell line)-derived conditioned media for 24 h. RANKL mRNA was significantly upregulated in osteoblasts ($P < 0.001$), with a significant reduction in OPG mRNA compared to negative controls ($P < 0.0001$) (Figure 4A). Next, conditioned media collected from primary CAFs was used to treat HOB osteoblasts. A significant increase in RANKL mRNA ($P < 0.03$) could be seen in osteoblasts after 48 h (Figure 4A).

TGF-β1 stimulates RANKL expression in primary fibroblasts. We next sought to determine if experimentally derived myofibroblastic CAF secrete RANKL. Previous work in our laboratory has indicated that treatment of normal primary oral fibroblasts with TGF-β1 provokes differentiation to a CAF-like, αSMA-positive phenotype (Melling *et al*, in submission). Primary oral fibroblasts were, therefore, treated with human recombinant TGF-β1 (5 ng ml^{-1}) for 72 h and differentiation to a CAF-like myofibroblastic phenotype was determined by examining the expression of αSMA protein, which increased significantly in response to TGF-β1 treatment (Figure 4B). Conditioned media was collected from control fibroblasts and TGF-β1-treated CAF-like fibroblasts and RANKL secretion examined by ELISA. TGF-β1 treatment resulted in a significant upregulation of RANKL in the conditioned media (Figure 4C, $P < 0.05$). Conditioned media from serum starved OSCC-derived CAF (three separate cultures) were collected and

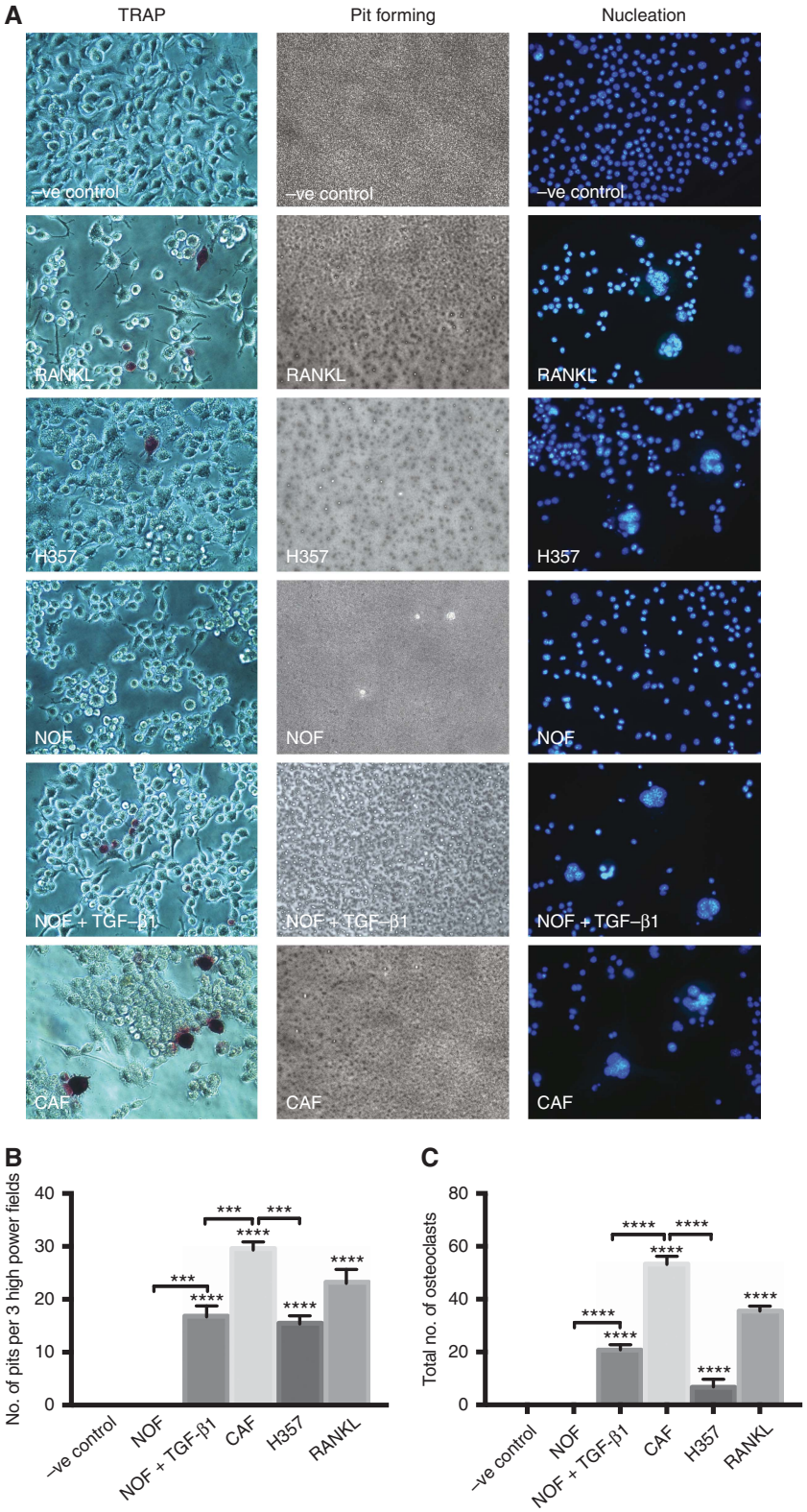

Figure 5. CAFs stimulate osteoclastogenesis *in vitro*. Conditioned media from serum starved H357 cancer cells, NOFs, TGFβ1-treated NOFs, and tumour-derived CAFs were collected and used to treat murine monocytes (RAW 264.7) cultured in a Corning Osteo assay 24-well plate. Monocytes were treated for 7 days with a daily media change. RANKL (50 ng ml^{-1}) served as a positive control, while serum-free differentiation media served as the negative control. (**A**) Representative photomicrographs showing TRAP staining, pit forming, and multinucleation (magnification $\times 40$). (**B**) Pit forming was evaluated and quantified per three high-power fields. (**C**) TRAP staining was quantified per well. Data represent $n = 3 \pm$ s.d. ***$P \leqslant 0.001$; ****$P \leqslant 0.0001$.

compared to media gathered from NOFs (three separate cultures) under identical conditions. RANKL secretion was quantified by ELISA and a significant increase in RANKL expression noted in CAF- compared to NOF-derived media (Figure 4D).

CAF directly promote osteoclastogenesis. Given the ability of experimentally derived CAF to generate and secrete RANKL (and other osteoclastogenic factors such as IL-6 and MCP-1 (Kabir *et al*, 2016)), we next sought to examine the effect of CAF-derived conditioned medium on osteoclastogenesis. Both experimentally derived CAF and primary CAF-derived from OSCC, as well as OSCC-derived cancer cells, were able to induce tartrate-resistant acid phosphatase (TRAP) (Figure 5A and B) pit formation in a synthetic bone substrate and multinucleation of macrophages (Figure 5A and C) at a significantly higher level than normal fibroblasts. Surprisingly, the effect of CAF on osteoclastogenesis was markedly greater than OSCC-derived cancer cells (Figure 5A–C).

DISCUSSION

OSCC has a high tendency to invade proximal bone, a feature conferring significant morbidity and a poor prognosis (Nomura *et al*, 2005). In this study, we aimed to examine the extent to which the tumour microenvironment, and in particular CAF, influence bone invasion. The presence of prominent stroma in bone invasive OSCC has previously been reported, but these were largely observational studies lacking robust experimental interrogation of functional CAF or clinicopathological correlation (Wong *et al*, 2000; Ebrahimi *et al*, 2011; Fried *et al*, 2014). We sought to examine the association between stroma and bone invasion in more detail and have identified for the first time a prominent functional role for CAF in bone invasive OSCC.

A discohesive invasion pattern for OSCC is known to be associated with a more destructive behaviour (Totsuka *et al*, 1991; Ishikuro *et al*, 2008; Ebrahimi *et al*, 2011). This was consistent with our observation that the advancing tumour front, when in close proximity to or invading bone tissue, was of a discohesive nature. In addition, osteoclast count in OSCC was significantly higher than ameloblastoma, suggesting higher bone turnover and resorption in OSCC similar to previous findings (Ishikuro *et al*, 2008). Interestingly, in the majority of cases analysed in our cohort, no direct contact between tumour and bone was evident, with abundant fibrous and variably desmoplastic stroma present at the OSCC tumour-bone interface. This contrasted with ameloblastoma, in which thick bundles of hyalinised collagen were present between tumour islands and bone with minimal αSMA staining.

A strong correlation between the presence of αSMA-positive stromal CAFs and poor patient outcome has been reported in a range of malignancies including breast (Surowiak *et al*, 2007), colorectal (Tsujino *et al*, 2007) and oesophageal (Saadi *et al*, 2010) carcinomas, as well as OSCC (Vered *et al*, 2010; Marsh *et al*, 2011). In our study, strong αSMA expression was seen in fibrous stroma of all bone invasive OSCC samples. In numerous cases, αSMA fibroblasts were noted visibly infiltrating bone, ahead of the epithelial tumour component, strongly supporting our hypotheses that a myofibroblastic stroma plays a crucial role in bone invasive OSCC. In contrast, ameloblastoma, a benign/locally invasive odontogenic tumour, only showed sporadic and weak αSMA staining in fibroblasts.

It has been suggested that the disequilibrium in osteolytic RANKL and OPG expression enhances progression of bone-associated malignancies (Jimi *et al*, 2013). We have shown that in addition to bone cells, tumour cells and fibrous stroma, as well as CAF in culture, express RANKL and OPG. Although some studies have shown RANKL expression in tumour cells in close proximity to bone (Ishikuro *et al*, 2008; Chaung *et al*, 2009; Kayamori *et al*, 2010), reports of OPG expression are variable and the absence of expression has also been reported in one study (Ishikuro *et al*, 2008). However, a recent study has reported OPG upregulation in bone invasive OSCC (Russmueller *et al*, 2015) suggesting that enhanced OPG expression depletes TNF-related apoptosis-inducing ligand (TRAIL) -induced cell apoptosis, hence promoting survival of tumour cells, which may explain the readily detectable levels of OPG in the stroma observed here.

Osteoblasts cultured with conditioned media from OSCC cells showed elevated RANKL expression and reduced OPG levels, in agreement with previous reports showing RANKL mRNA amplification and OPG reduction in BHY murine osteoblasts cultured with OSCC-conditioned media (Ishikuro *et al*, 2008). Our findings also show for the first time that OSCC-derived CAF and experimentally derived CAF-like fibroblasts are able to invoke similar responses in osteoblasts, suggesting that CAF may play a functional role in bone remodelling in OSCC.

Bone destruction and OSCC invasion requires the generation of osteoclasts (multinucleated bone resorbing cells) originating from monocyte/macrophage lineage haematopoietic precursors. It has been previously reported that exposure to RANKL facilitates osteoclastogenesis in the murine macrophage cell line RAW 264.7 (Vincent *et al*, 2009), and a similar effect is seen in response to cancer-cell-derived factors. This was corroborated by our findings obtained with OSCC-cell-derived conditioned media. Interestingly, we also observed a significantly greater stimulation of osteoclastogenesis following incubation of RAW 264.7 cells in conditioned media from CAF (OSCC-derived and experimentally derived) with morphological transdifferentiation after 5 days, TRAP positivity within 7 days and pit formation on osteo-surface wells (Halleen *et al*, 2000).

In conclusion, our data provide, for the first time, *ex vivo* and *in vitro* evidence that CAF have a key role in bone invasion in OSCC manipulated through a RANKL-dependent pathway. This suggests that stromal factors may hold promise as novel therapeutic targets in bone invasive OSCC.

ACKNOWLEDGEMENTS

We thank Helen Colley, Alasdair McKechnie, Keyvan Moharamzadeh, Amy Harding and Thafar Almeda for providing primary cells, Brenka McCabe and David Thompson for technical support, and Alison Gartland for helpful discussions.

CONFLICT OF INTEREST

The authors declare no conflict of interest.

AUTHOR CONTRIBUTIONS

AAE and AEP performed experiments, AAE, AEP, SAK and DWL performed data analyses, AAE, SAK and DWL wrote the manuscript, SAK and DWL devised and designed the study. All authors have read and approved the manuscript.

REFERENCES

Chen Y, Kuo S, Fang K, Hao S (2011) Prognostic impact of marginal mandibulectomy in the presence of superficial bone invasion and the nononcologic outcome. *Head Neck* **33**: 708–713.

Chuang F, Hsue S, Wu C, Chen Y (2009) Immunohistochemical expression of RANKL, RANK, and OPG in human oral squamous cell carcinoma. *J Oral Pathol Med* **38**: 753–758.

De Wever O, Demetter P, Mareel M, Bracke M (2008) Stromal myofibroblasts are drivers of invasive cancer growth. *Int J Cancer* **123**: 2229–2238.

Ebrahimi A, Murali R, Gao K, Elliott M, Clark J (2011) The prognostic and staging implications of bone invasion in oral squamous cell carcinoma. *Cancer* **117**: 4460–4467.

Fried D, Mullins B, Weissler M, Shores C, Zanation A, Hackman T, Shockley W, Hayes N, Chera B (2014) Prognostic significance of bone invasion for oral cavity squamous cell carcinoma considered T1/T2 by American joint committee on cancer size criteria. *Head Neck* **36**: 776–781.

Halleen J, Alatalo S, Suominen H, Cheng S, Janckila A, Väänänen H (2000) Tartrate–resistant acid phosphatase 5b: a novel serum marker of bone resorption. *J Bone Miner Res* **15**: 1337–1345.

Hearnden V, Lomas H, MacNeil S, Thornhill M, Murdoch C, Lewis A, Madsen J, Blanazs A, Armes S, Battaglia G (2009) Diffusion studies of nanometer polymersomes across tissue engineered human oral mucosa. *Pharm Res* **26**: 1718–1728.

Hinsley EE, Hunt S, Hunter KD, Whawell SA, Lambert DW (2012) Endothelin-1 stimulates motility of head and neck squamous carcinoma cells by promoting stromal-epithelial interactions. *Int J Cancer* **130**: 40–47.

Ishikuro M, Sakamoto K, Kayamori K, Akashi T, Kanda H, Izumo T, Yamaguchi A (2008) Significance of the fibrous stroma in bone invasion by human gingival squamous cell carcinomas. *Bone* **43**: 621–627.

Jimi E, Shin M, Furuta H, Tada Y, Kusukawa J (2013) The RANKL/RANK system as a therapeutic target for bone invasion by oral squamous cell carcinoma (Review). *Int J Oncol* **42**: 803–809.

Kabir T, Leigh R, Tasena H, Mellone M, Coletta R, Parkinson E, Prime S, Thomas G, Paterson I, Zhou D, McCall J (2016) A miR-335/COX-2/PTEN axis regulates the secretory phenotype of senescent cancer-associated fibroblasts. *Aging (Albany NY)* **8**: 1608.

Kayamori K, Sakamoto K, Nakashima T, Takayanagi H, Morita K, Omura K, Nguyen S, Miki Y, Iimura T, Himeno A, Akashi T (2010) Roles of interleukin-6 and parathyroid hormone-related peptide in osteoclast formation associated with oral cancers: significance of interleukin-6 synthesized by stromal cells in response to cancer cells. *Am J Pathol* **176**: 968–980.

Khurram S, Whawell S, Bingle L, Murdoch C, McCabe B, Farthing P (2010) Functional expression of the chemokine receptor XCR1 on oral epithelial cells. *J Pathol* **221**: 153–163.

Livak K, Schmittgen T (2001) Analysis of relative gene expression data using real-time quantitative PCR and the $2-\Delta\Delta CT$ method. *Methods* **25**: 402–408.

Marsh D, Suchak K, Moutasim K, Vallath S, Hopper C, Jerjes W, Upile T, Kalavrezos N, Violette S, Weinreb P, Chester K (2011) Stromal features are predictive of disease mortality in oral cancer patients. *J Pathol* **223**: 470–481.

Müller H, Slootweg P (1990) Mandibular invasion by oral squamous cell carcinoma: clinical aspects. *J Craniomaxillofac Surg* **18**: 80–84.

Nomura T, Shibahara T, Cui N, Noma H (2005) Patterns of mandibular invasion by gingival squamous cell carcinoma. *J Oral Maxillofac Surg* **63**: 1489–1493.

Quan J, Johnson N, Zhou G, Parsons P, Boyle G, Gao J (2012) Potential molecular targets for inhibiting bone invasion by oral squamous cell carcinoma: a review of mechanisms. *Cancer Metastasis Rev* **31**: 209–219.

Radisky D, Kenny P, Bissell M (2007) Fibrosis and cancer: do myofibroblasts come also from epithelial cells via EMT? *J Cell Biochem* **101**: 830–839.

Roland N, Caslin A, Nash J, Stell P (1992) Value of grading squamous cell carcinoma of the head and neck. *Head Neck* **14**: 224–229.

Russmueller G, Moser D, Würger T, Wrba F, Christopoulos P, Kostakis G, Seemann R, Stadler V, Wimmer G, Kornek G, Psyrri A (2015) Upregulation of osteoprotegerin expression correlates with bone invasion and predicts poor clinical outcome in oral cancer. *Oral Oncol* **51**: 247–253.

Saadi A, Shannon N, Lao-Sirieix P, O'Donovan M, Walker E, Clemons N, Hardwick J, Zhang C, Das M, Save V, Novelli M (2010) Stromal genes discriminate preinvasive from invasive disease, predict outcome, and highlight inflammatory pathways in digestive cancers. *Proc Natl Acad Sci USA* **107**: 2177–2182.

Surowiak P, Murawa D, Materna V, Maciejczyk A, Pudelko M, Ciesla S, Breborowicz J, Murawa P, Zabel M, Dietel M, Lage H (2007) Occurrence of stromal myofibroblasts in the invasive ductal breast cancer tissue is an unfavourable prognostic factor. *Anticancer Res* **27**: 2917–2924.

Totsuka Y, Usui Y, Tei K, Fukuda H, Shindo M, Lizuka T, Amemiya A (1991) Mandibular involvement by squamous cell carcinoma of the lower alveolus: analysis and comparative study of histologic and radiologic features. *Head Neck* **13**: 40–50.

Tsujino T, Seshimo I, Yamamoto H, Ngan C, Ezumi K, Takemasa I, Ikeda M, Sekimoto M, Matsuura N, Monden M (2007) Stromal myofibroblasts predict disease recurrence for colorectal cancer. *Clin Cancer Res* **13**: 2082–2090.

Vered M, Dayan D, Yahalom R, Dobriyan A, Barshack I, Bello I, Kantola S, Salo T (2010) Cancer–associated fibroblasts and epithelial–mesenchymal transition in metastatic oral tongue squamous cell carcinoma. *Int J Cancer* **127**: 1356–1362.

Vincent C, Kogawa M, Findlay D, Atkins G (2009) The generation of osteoclasts from RAW 264.7 precursors in defined, serum-free conditions. *J Bone Miner Metab* **27**: 114–119.

Wong R, Keel S, Glynn R, Varvares M (2000) Histological pattern of mandibular invasion by oral squamous cell carcinoma. *Laryngoscope* **110**: 65–72.

Supplementary Information accompanies this paper on British Journal of Cancer website (http://www.nature.com/bjc)